The mode of deformation in the orogenic mid-crust revealed by seismic attribute analysis

Taija Torvela
Department of Geology and Petroleum Geology, University of Aberdeen, UK

Department of Geosciences and Geography, University of Helsinki, Finland

School of Earth and Environment, University of Leeds, UK (t.m.torvela@leeds.ac.uk)

Julien Moreau, Annakaisa Korja, and Pekka Heikkinen
Department of Geosciences and Geography, University of Helsinki, Finland

Robert W. H. Butler
Department of Geology and Petroleum Geology, University of Aberdeen, UK

[1] The processes and the structures within the middle and the lower crust are intimately related to the evolution of orogenies, but more detailed knowledge is needed of these deep crustal processes. Seismic reflection data, chiefly displayed in amplitude, are commonly used to interpret deep crustal structures. The strongest amplitude events are probably related to lithological changes and do not necessarily correspond to geological structures, tectonic boundaries, or deformation fabrics. Furthermore, the detailed structures and the strain distribution between the interpreted structural boundaries remain obscure. Here, we show an example of how seismic attributes, combined with the seismic facies interpretation technique, can be used to enhance 2D seismic reflection data from the Palaeoproterozoic Svecofennian crust of southern Finland, to reveal unprecedentedly detailed information about the deformation fabrics within the mid-crust of a collisional orogen. The images are plausibly interpreted to show that the extension/lateral flow of the orogenic middle and lower crust was mainly accommodated by kilometer-scale S-C′ structures. The structures form penetrative deformation fabrics which are correlated with outcrop observations. The successful enhancement of the seismic data confirms the ductile extension affecting hot orogenic crust, and gives new information about the strain distribution of the regional, syn- to late-orogenic deformation. The seismic attribute method and the seismic facies interpretational approach described in this paper should be applicable to other seismic datasets from the crystalline basement.

1. Introduction

[2] Understanding the deep crustal structure of orogenic belts has always been a major challenge for Earth scientists. A variety of geophysical approaches is used to extrapolate geology seen at outcrop into the deeper crust. One principal tool has been seismic reflection [e.g., *Choukroune and ECORS team*, 1989; *Clowes et al.*, 1992; *Klemperer and Hobbs*, 1991; *Nelson et al.*, 1996]. Crustal seismic data are conventionally displayed with wiggles and strong peak amplitudes only, and the kilometer-scale patterns of distinct, continuous reflection events are interpreted as geological structures. However, large amplitude changes observed on crustal seismic reflectivity are usually interpreted to arise from lithological changes, but these changes may or may not correspond to structural boundaries [e.g., *Rutter et al.*, 1999]. Furthermore, the resolution of this display method usually only allows mapping of large-scale features, such as terrane-scale crustal shear and fault zones, Moho, intrusions, and basin geometries [e.g., *Drummond et al.*, 2000; *Fernández-Viejo et al.*, 2011; *Korja and Heikkinen*, 1995]. Consequently, very little is imaged of the more detailed, in situ, sub-kilometer-scale structural geometries and strain distribution, and therefore, the causal deformation processes within the middle and lower crust remain partly unresolved. More advanced seismic data interpretation techniques are needed in order to enhance the structural interpretation. There are undeniable physical restrictions to the usage of 2D data and to the scale to which seismic reflection data can be resolved, but observation of sub-kilometer scale features should be achievable.

[3] Seismic interpretation can be enhanced by using so-called seismic attributes. Seismic attributes essentially represent any characteristic that can be calculated from the measured seismic signal and used to illustrate specific rock properties [e.g., *Barnes*, 2001; *Taner*, 2001; *White*, 1991]. Attributes range from "simple" 1D statistical descriptions of the signal geometry [e.g., instantaneous attributes; *White*, 1991] to specific multi-trace signal properties [e.g., spectral decomposition, dip, waveform, curvature; *Barnes*, 2001]. Various attributes are routinely used in the petroleum industry to enhance seismic data from sedimentary basins, for both regional-scale and sub-kilometer scale interpretation. Seismic attribute analysis has revolutionized the understanding of sedimentary facies and the related epositional architectures now buried in the subsurface [e.g., *Randen and Sønneland*, 2005; *Taner*, 2001]. Seismic attributes are also increasingly being used to enhance and detect detailed deformation fabrics and strain distribution within the strata [e.g., *Iacopini and Butler*, 2011].

[4] In the analysis of data from the crystalline continental lithosphere, a number of attributes were tested in the pioneering works related to the large consortium projects in the 1980s–1990s (e.g., LITHOPROBE, BIRPS, ECORS, DEKORP, TRANSALP). Intense discussions followed on the applicability of filtering, using attributes, on 2D seismic data to enhance imaging of the crust [e.g., *Levander et al.*, 1994]. Based on empirical estimations of physical properties of basement rocks and forward modelling, it has been argued that strong diffraction and scattering of the signal is inevitable in anisotropic rocks at depth (>4 s TWT), rendering the ray theory approximations inadequate [e.g., *Holliger et al.*, 1994; *Levander et al.*, 1994]. Consequently, objects smaller than 1 km cannot be resolved at great depths [*Levander et al.*, 1994]. The depth of observation of filtered data is, in other words, critical. While the reliable application of attributes and filters for detailed interpretation of 2D data was controversial, many attributes, perhaps most notably the various coherency filters, were used with some success to enhance imaging of the deep crust at a kilometer-scale [e.g., *Eaton and Cook*, 1988; *Fertig et al.*, 1999; *Meissner and Bortfeld*, 1990; *Rey*, 1993; *Taner et al.*, 1979]. However, the spectrum of the available seismic attributes has dramatically increased over the last 10–15 years, facilitated by the constantly increasing computing power, access to software, and the resulting ease of data visualization, while at the same time the quality of the acquired seismic (2D) data has improved. Although many of the "new" attributes, now routinely used to image 3D data, may not be appropriate for 2D data from the crystalline basement, most of them have not yet been tested.

[5] In orogenic belts, crustal thickening precedes rheological weakening of the middle and lower orogenic crust [e.g., *Beaumont et al.*, 2001; *Royden et al.*, 1997; *Rey et al.*, 2001]. The mode of deformation and the resulting strain distribution within the weakened crust have attracted increasing attention since the first published models for mid-crustal flow and synorogenic extension [e.g., *Beaumont et al.*, 2001; *Coney and Harms*, 1984; *Royden et al.*, 1997; *Vanderhaege and Teyssier*, 2001]. In modern orogenies, the middle and lower crust are locally, but not everywhere, exposed. Important insights into the syn- to post-orogenic processes within the deep crust can, therefore, be gained by studying the exposed roots of old, eroded orogenies. Our case study

area comes from the exhumed, migmatitic mid-crust of a Palaeoproterozoic orogen in southern Finland. At outcrop, it contains ubiquitous, subhorizontal to gently dipping structures (e.g., foliations, stretching lineations, fold axial planes), together with moderately to steeply dipping narrow zones of highly strained rocks interpreted as major tectonic boundaries and local shear zones. The crust is imaged by the Finnish Reflection Experiment (FIRE) that was designed to image the major crustal structures in Finland. The FIRE data have been previously interpreted in terms of the major crustal structures and terrane boundaries [e.g., *Nironen et al.*, 2006]. However, major uncertainty exists as to how strain is distributed during orogenic extension or lateral flow in general, and to what degree the resulting structures are represented in the seismic data and by the deformation fabrics observed at outcrop. The frequently observed and widespread distribution of intensely deformed rocks at outcrop suggests that the strain was widely distributed within the crust during orogenesis and the related extension/crustal flow, rather than localizing onto narrow shear zones. Thus, the in situ detection of these fabrics is important for a more accurate quantification of the orogenic processes and, consequently, for more geologically realistic models of the development of orogenic belts.

[6] The aim of this paper is to apply seismic attribute analysis to enhance structural interpretation of the crystalline basement, especially to detect sub-kilometer scale deformation fabrics at depth. A multi-trace attribute (dip-steering median filter) is applied on seismic data from the case study area, in order to investigate the strain distribution during syn-orogenic extension. After providing brief notes on the field setting, on the nature of the deformation at outcrop, and on the seismic project, we describe the method used for enhancing the seismic data. The orientations of the crustal structures, interpreted from the filtered data, are related to those seen at outcrop, extrapolating these into a model of crustal deformation. Finally, the approach and the interpretation are discussed in the context of the applicability of the ray theory to the data, and of general deformation models for continental orogenic crust.

2. Geological Setting and Outcrop Structure

[7] The case study area is located in the Palaeoproterozoic Svecofennian orogenic crust in southern Finland (the West Uusimaa area; Figure 1). "Svecofennian" refers collectively to the basement rocks in present Finland, Sweden, Karelia (NE Russia), and Estonia that formed during multiple orogenic events between c. 2.0 and 1.79 Ga [*Gaál and Gorbatschev*, 1987]. The Svecofennian is currently divided into three or four separate orogenies: the Fennian orogen at c. 2.0–1.85 Ga [which may have consisted of two separate orogenic events; *Rutland et al.*, 2004], the Andean-type Svecobaltic orogen at c. 1.84–1.80 Ga, and the Nordic orogen with a continent-continent collision at 1.82–1.79 Ga [Figure 1; *Lahtinen et al.*, 2005]. Most of the igneous and sedimentary rocks in central and southern Finland formed during the Fennian orogen, but experienced post-orogenic extension and basin development, followed by another phase of crustal thickening and deformation during the Svecobaltic orogen [e.g., *Lahtinen et al.*, 2005 and references therein].

[8] In southern Finland, the deepest exposure level occurs along an approximately E-W trending, c. 100 km wide, curvilinear "Late-Svecofennian Granite-Migmatite belt" LSGM [*Ehlers et al.*, 1993; Fig. 1a]. Along the exposed LSGM, the metamorphic grade is very close to the amphibolite-granulite facies transition [here, c. 15 km palaeodepth; e.g., *Väisänen and Hölttä*, 1999] where the orogenic crust is significantly rheologically weakened due to anatexis and migmatization [e.g., *Rey et al.*, 2009]. The crustal anatexis along the LSGM occurred in at least two, possibly three separate phases between c. 1.85–1.82 Ga [*Kurhila et al.*, 2005; *Skyttä and Mänttäri*, 2008]. One more anatectic phase may have taken place at c. 1.79 Ga [*Kurhila et al.*, 2011]. Approximately orogen-parallel (i.e., E-W), syn-orogenic mid-crustal flow similar to that in the modern Himalayas has been suggested to have occurred in southern Finland during this time, based on structural field data and analogue modelling [*Cagnard et al.*, 2007]. The modes and the strain distribution of the extension/flow within the weakened domain have, however, not yet been investigated.

[9] The West Uusimaa area in southern Finland is one of the key areas for deciphering the development and behavior of the Svecofennian orogenic middle crust (Figures 1b and 2). The area has historical importance: *Eskola* [1915] developed the concept and classification of metamorphic facies based on his observations of the rocks in West Uusimaa, while the migmatite nomenclature and basic formation concepts are based on the work of *Sederholm* [1926]. A number of geoscientists have since worked in the West Uusimaa area, revealing important information on the development and
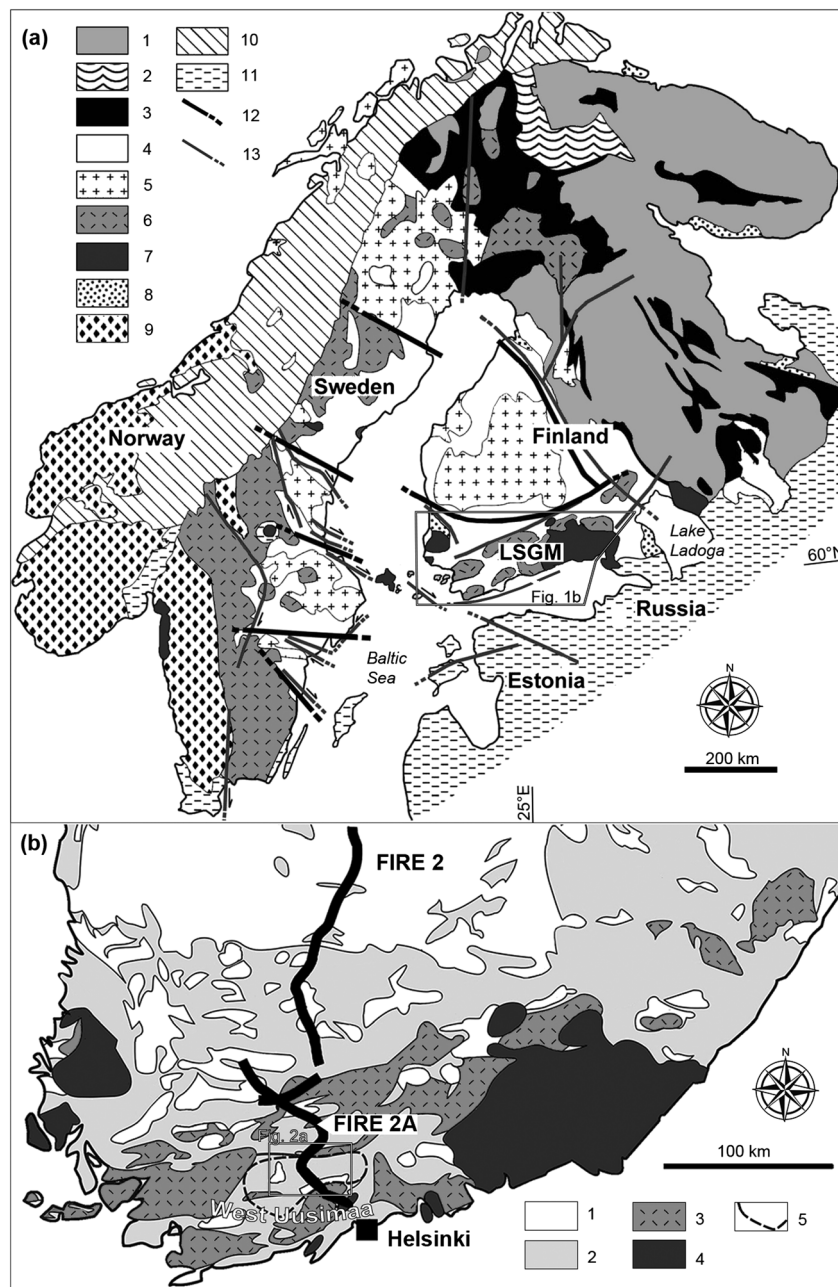
Figure 1. (a) Generalized geological map of the Fennoscandian shield. Key: **1** Archaean rocks 3.2–2.5 Ga; **2** Lapland granulite belt 2.2–1.9 Ga; **3** Karelian supracrustal rocks 2.5–1.9 Ga; **4** Granitoids, metasupracrustal gneisses, and migmatites of the Fennian orogeny 2.0–1.85 Ga; **5** Fennian pre- and synorogenic magmatic rocks 1.95–1.85 Ga; **6** Syn- and post-Svecobaltic and Nordic granites and migmatites 1.85–1.77 Ga; **7** Anorogenic rapakivi granites 1.65–1.4 Ga; **8** Sandstones, Jotnian and younger 1.5–0.57 Ga; **9** Sveconorwegian rocks 1.25–0.9 Ga; **10** Caledonian rocks 0.6–0.4 Ga; **11** Phanerozoic sedimentary cover <0.57 Ga; **12** Domain/terrane borders; **13** Major Palaeoproterozoic deformation zones; LSGM = Late Svecofennian Granite Migmatite zone. Modified from *Korsman et al.* [1997]. (b) Generalized geological map of southern Finland. Key: **1** Svecofennian granitoids; **2** Svecofennian metasupracrustal gneisses and migmatites; **3** Late-Svecofennian granites and migmatites; **4** Anorogenic rocks; **5** Pyroxene-in boundary of the WUC. Modified from *Nironen et al.*, 2006.

behavior of the Svecofennian middle crust [e.g., *Cagnard et al.*, 2007; *Mouri et al.*, 2005; *Nironen et al.*, 2006; *Pajunen et al.*, 2008; *Schreurs and Westra*, 1986; *Skyttä and Mänttäri*, 2008; *Stel et al.*, 1989].

[10] In the northern part of the West Uusimaa area, the mid-crustal rocks are exposed within a dome-like structure, the West Uusimaa Complex [WUC; Figure 2; e.g., *Schreurs and Westra*, 1986]. The WUC metavolcanics and metasediments formed in a

back-arc setting, and were multiply folded, migmatized, and metamorphosed in granulite facies conditions during the Svecobaltic orogeny [Figures 3a–c; e.g., *Schreurs and Westra*, 1986]. The metavolcanics and metasediments have been intruded by relatively undeformed, mostly granodioritic, pyroxene-bearing rocks (Figure 3c). The structures define large-scale dome-and-basin geometries [e.g., *Ehlers et al.*,

1993]. The WUC is surrounded by lower-grade crustal blocks: sharp boundaries to these blocks are observed in the north and in the west [the late- to post-orogenic Somero-Karkkila and Suomusjärvi fault zones; Figure 2b; e.g., *Schreurs and Westra*, 1986], while to the east and the south, the boundaries are gradational, defined by the pyroxene-in isograd (Figure 2b). The WUC, along with the rest of the
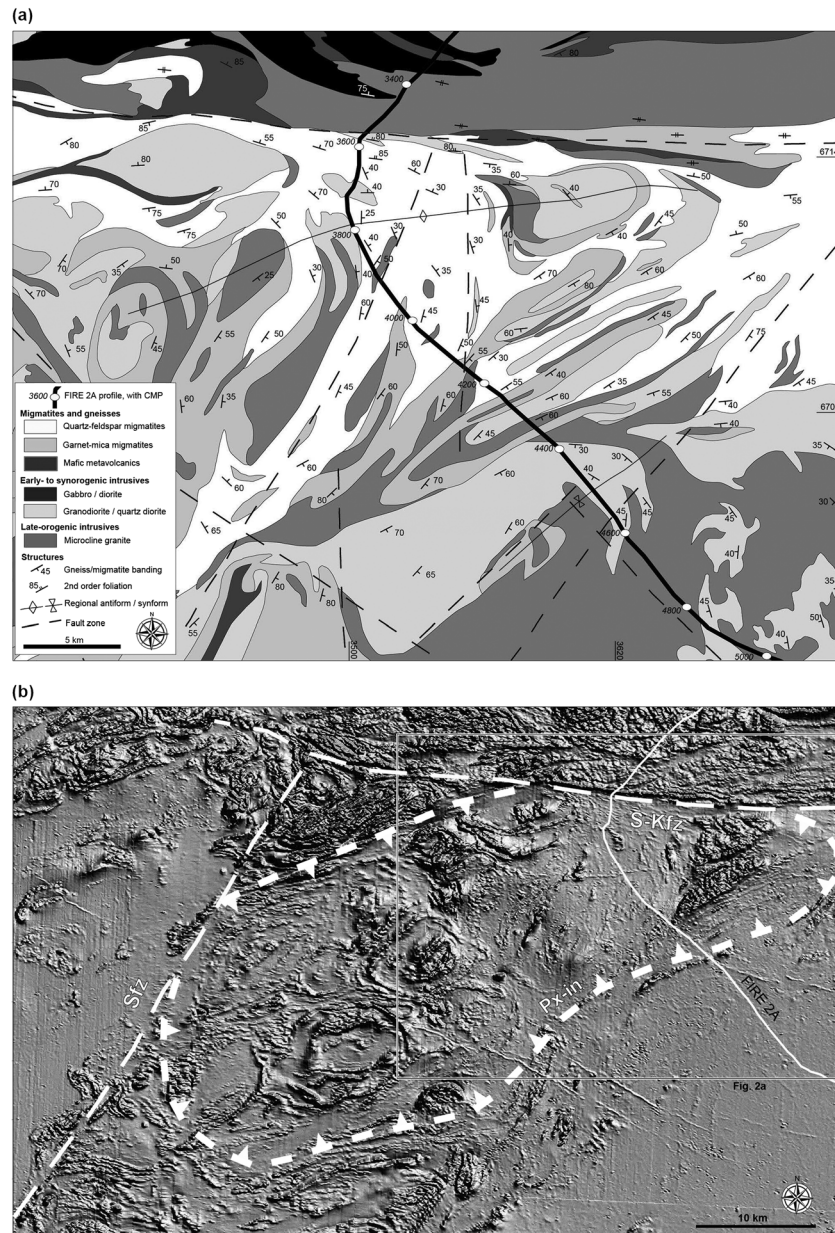

Figure 2. (a) Generalized geological map of the study area (coordinates ETRS-TM35FIN). FIRE 2A line with CMPs is indicated. The "2nd order foliation" refers to foliations overprinting the migmatitic and gneissose banding, i.e., younger deformation. The map is based on the Geological survey of Finland 1:100,000 map of Pre-Quaternary rocks, updated with more detailed field data along and in the vicinity of the FIRE 2A profile. (b) Aeromagnetic map of the WUC and neighboring areas. The fault zones bounding the WUC and the pyroxene-in isograd are indicated. A regional-scale, low-altitude aeromagnetic shaded relief image (black maximum, white minimum), illumination from the upper right-hand corner. Map courtesy of Geological Survey of Finland.
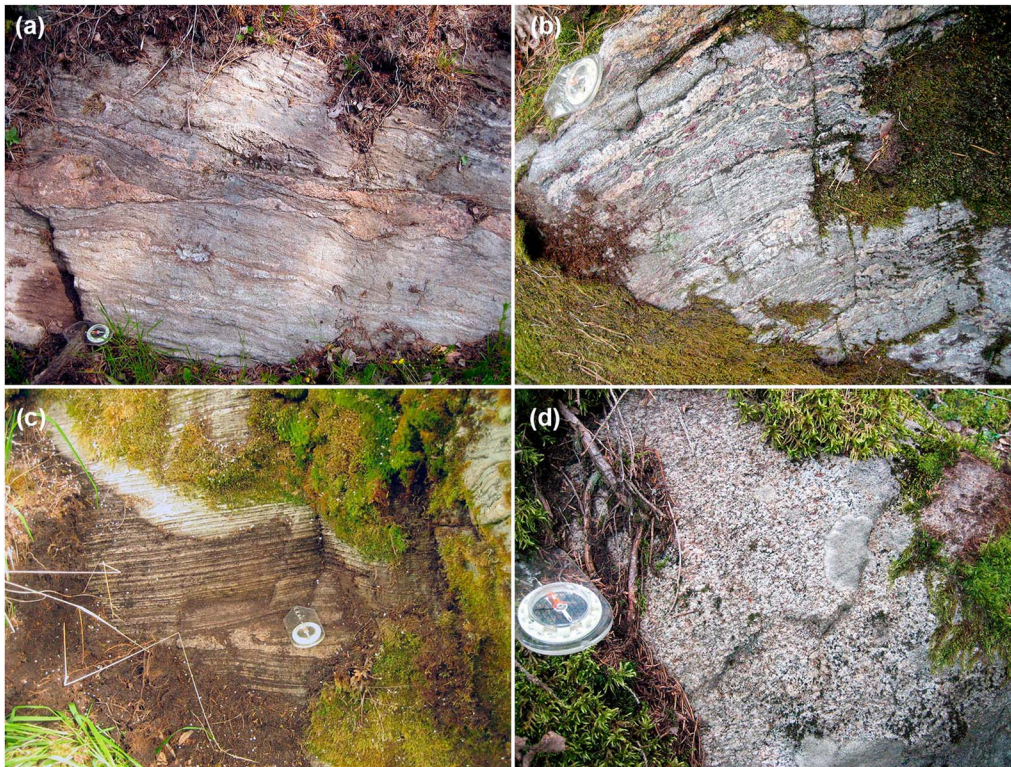
Figure 3. Typical rocks within the WUC (see also Figure 2a). (a) Quartz-feldspar migmatites. The mafic mineral is usually amphibole, sometimes biotite is present. The rocks are characterized by abundant leucosomes, and granitic dykes and veins that are often boudinaged or folded. (b) Garnet-mica migmatites. The mica is sometimes replaced by amphibole, and the rocks are locally cordierite-bearing. Also these rocks contain abundant leucosomes and dykes/veins. (c) Intensely sheared (two-)pyroxene bearing felsic granulites. The rocks consist mainly of plagioclase, feldspar, quartz, pyroxene (mostly diopside, sometimes also hypersthene), and titanite, with occasional crystalline calcite. Despite the intense shearing, the rocks have been completely statically recrystallized, so that kinematic markers are extremely rare and the internal strain of the individual grains is very low (in thin section; not shown). These shear zones, where observed at outcrop, correlate with shear zones interpreted in the seismic data (Figure 8). (d) Early- to synorogenic intrusives that are usually of granodioritic to quartz-dioritic composition and often contain hypersthene. The rocks are clearly foliated, the foliation orientations being consistent with the banding patterns of the surrounding migmatites, but are much less deformed than the migmatites.

LSGM, is structurally overlain by subhorizontal sheets of weakly deformed or undeformed anatectic microcline granites that are interpreted to have intruded late- to post-kinematically into the surrounding migmatites and gneisses [e.g., *Ehlers et al*., 1993; *Kurhila et al*., 2005; Figure 1]. This paper focuses on the northeastern part of the WUC which is imaged by the FIRE deep seismic reflection experiment (line FIRE 2A; Figures 1b and 2). The large-scale crustal features along the FIRE 2A have been preliminarily interpreted by *Nironen et al.* [2006] who suggest extension along large-scale shear zones (apparent extension along the 2D profiles toward the SE). The geological maps of the area are relatively low-resolution (1:100,000; Geological Survey of Finland). More detailed field work has been carried out for the purposes of this paper in the vicinity of the FIRE 2A profile, and the geological map was updated where necessary (Figure 2a). The number and the quality of the exposures in many places are relatively poor, due to the low relief and the presence of Quaternary sedimentary cover, but the main geological features remain mappable. The observed structures within the study area, i.e., the dome and the related shear zones and folds within the WUC, are at or above the scale theoretically resolvable by the FIRE seismic reflection data (characteristic scales of 100–1000 m; Figure 2).

3. Seismic Reflection Data

3.1. Acquisition

[11] The seismic reflection data were acquired during the Finnish Reflection Experiment (FIRE)

in 2001–2005 [*Kukkonen et al.*, 2006]. The entire experiment covers altogether 2104 km of 2D survey lines, transecting all the major geological units in Finland. The signal was generated using Vibroseis sources, mostly on asphalt-covered public roads. The acquisition had a split-spread geometry with 362 geophone groups with 50 m intervals (mean offset 9 km, maximum offset 18 km). The acquisition parameters are listed in Appendix I.

3.2. Processing

[12] Data processing was done in three parts (Appendix I). The field quality control included the static corrections, with the production of brute stacks. The residual statics, finals stacks and the first migrated results were done after the field work by the contractor [*Zamoshnyaya and Suleimanov*, 2003]. The final migration and the depth conversion were performed at the Institute of Seismology, University of Helsinki. The migration was done on the stacked data with Stolt-migration, using a 1D velocity model based on the SVEKA'81 refraction soundings [*Grad and Luosto*, 1987]. NMO (normal move-out) stacks with full record length of 30 s were prepared. The depth conversion is based on the 1D velocity model (Appendix I). The velocities between the fixed depths were calculated by linear interpolation. The final amplitude image from the case study area (FIRE 2A, CMPs 3300–5000) is shown in Appendix II in the Supporting Information.[1]

[13] After processing, the 2D seismic lines have a bin spacing of 25 m for a vertical sampling rate of 2 ms. The data are of a very high quality; a good signal penetration and high signal-noise ratios were maintained to at least 20 s TWT (two-way-travel time), corresponding to depths of 60–70 km. Band-pass filter analysis of the NMO stacks reveals that frequencies of up to 60 Hz are present throughout the depth range of the crust (15–17 seconds TWT), and that the entire bandwidth of 12–80 Hz is present in the upper crust. Considering the velocity model and a central frequency of 60 Hz, the vertical resolution of the FIRE data is theoretically c. 25×50 m throughout the crust [vertical × horizontal; *Kukkonen et al.*, 2006]. The real resolution and, therefore, the detectability of objects is partly dependent of the scattering regime of the signal. In this paper, the FIRE data are filtered and interpreted down to 15 km depth: within this interval, the signal falls dominantly into the optical regime where ray the-

ory is applicable [*Wu and Aki*, 1988; Figure 4a). Consequently, in absence of visible hyperbola or similar artifacts, it is plausible to consider that the observed coherent reflections across multiple traces image real objects and are not the product of scattering interaction patterns. The coherency of the reflections and, therefore, the reliability of the detection of reflection continuity is further enhanced by the filter described in the following chapter.

4. Methodology: The Seismic Attribute Approach

[14] A multi-trace geometric attribute, the dip attribute, was tested for guiding (steering) the amplitudes between traces. The dip-steered median filter of OpendTect (dGB software, academic licence) was found to be very efficient in enhancing the structural geometries in the FIRE2A data. The method and the workflow are described in detail at the OpendTect online resources pages (links in Acknowledgments; see also *Brouwer and Huck*, 2011]. The workflow initiates with the calculation of the apparent mean reflection dip within a user-specified window covering several traces and samples (here, a window size of 9 traces by 9 samples, i.e., c. 225 m × 112.5 m, was used). To calculate the apparent mean reflection dip within the plane of the seismic profile, a standard fast Fourier transform is performed for each trace (OpendTect algorithm, included in the academic licence). The computed peak frequencies and their spatial positions are compared between the traces within the chosen window, allowing the calculation of the mean (apparent) dip. The dips have then been smoothed with a window size of 225×300 m. The first 0–312.5 m from the Earth's surface are absent on the filtered data due to computation limitations of the filter: the first dip smoothing window has no comparison upwards, so that the values cannot be computed for the uppermost samples. The result is an estimation of the relative apparent 2D structural dip along the seismic line at the chosen resolution between 312.5 m and 15 km (Appendix II in the supplementary material). In the NMO migrated FIRE2A data, the calculated dips of the reflections range mainly between ±25° (Figures 4b and 4c). The second stage begins with calculating the filtered amplitudes, sample by sample, along each trace. Each amplitude value consists of the median value calculated for the sample and the extrapolated amplitude values of the two neighboring traces, along the calculated structural dip. Edge effects have been allowed so that in case of a phase

---

[1] All Supporting Information may be found in the online version of this article.
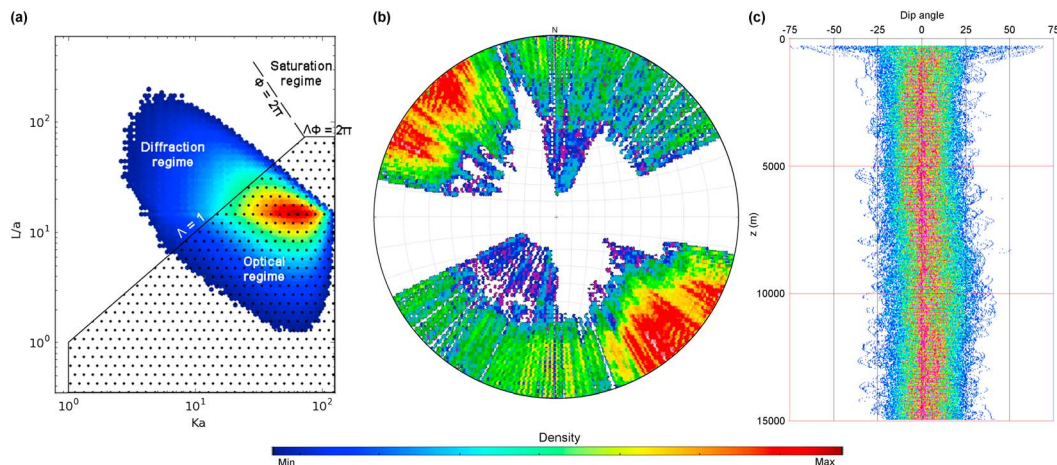
Geochemistry Geophysics Geosystems G³

Figure 4. Quality check diagrams for the filtering results of FIRE2A. (a) Transmission regime diagram of the studied interval (0.35–15 km) for subkilometric elements using the method of *Wu and Aki* [1988]. The diagram illustrates that most of the data are within the optical regime where the ray theory and its parabolic approximation are valid (dotted area). A minor part of the data is in the diffraction regime where artefacts might be expected. For details, see *Wu and Aki* [1988]. a = scale length of the heterogeneities; L = propagation length of the wave; k = the wavenumber. k is evaluated from the bandwidth sampled by the frequencies f, for a velocity v of 6 km/s ($k = 2\pi f/v$). L, f, and a vary within 350–15000 m, 6–120 Hz, and 25–1000 m, respectively. The limits between the different regimes are obtained by considering the diffraction parameter Λ, and the scattering strength parameter Φ, where $(\Lambda \Phi)^{0.5} > 1\%$. (b) Equal angle lower hemisphere projection of the pole of the dips along the FIRE2A profile ($n = 2{,}257{,}920$). Note that the measured reflection dips are not normalized against the number of traces, so that the dip direction distribution is directly dependent on the orientation of the seismic line (mostly NW-SE). (c) Vertical distribution of the dips down to a depth of 15 km. The steep dips (>c. 50°) close to the surface are artificial, caused by the "excessive" migration at the processing stage of the subsampled reflections at the surface.

difference in one of the three traces being compared, the median calculation ignores the different value, thus allowing the preservation of discontinuities.

[15] The entire filtered section is presented in Appendix III, and the high-resolution image is downloadable from the Virtual Seismic Atlas (www.seismicatlas.org). Some more detailed examples of the results are presented in Figure 5. The median filter, applied to the FIRE 2A data, results in a significant enhancement of the continuity of the reflections. The dip-steering median filter is a two-fold method using the dip orientation information from numerous reflections and traces as a geometrical base for a small-scale smoothing of the reflections. The result is a filter that has distinct advantages compared to filters that extrapolate the signal between traces or between windows, or along extrapolated horizons with no consideration of the overall architecture. For example, it is superior to the various coherency filters, utilized especially in the 1980s–1990s [e.g., *Rey*, 1993]. The dip-steering median filter considers several traces/samples (here, 9×9) to first construct the local structural grain (dip) that determines which reflections are considered to be coherent in the second filtering step. Therefore, the dip-steering median filter does not

connect reflections that would define dips conflicting with the general structural grain. The two-step filtering process also has the advantage of preserving geologically significant reflection disruptions (faults and shear zones), and avoiding the horizontal smearing of the signal (excessive smoothing). The approach is fundamentally different from some filters (e.g., coherency) that determine the dip and the amplitude smoothing during a single step and at the same scale without passing through a deconvolution stage. The main problem with such filters is that, used at a small (kilometer to sub-kilometer) scale, they will include random noise as much as real signal into the dip determination; and if used at a large (kilometer to crustal] scale, they will smear the signal, removing most of the details. The dip-steering median filter, conversely, is not sensitive to random noise: random noise shows no coherent dip, enabling the median filter to remove or weaken the noise amplitudes. The quality check of the filtering results, i.e., the examination and comparison of the original and filtered data, reveals no deformation of the geometries. Consequently, compared to the original amplitude data, the structures are considerably enhanced, facilitating accurate seismic interpretation at sub-kilometric scale. It should, however, be emphasized
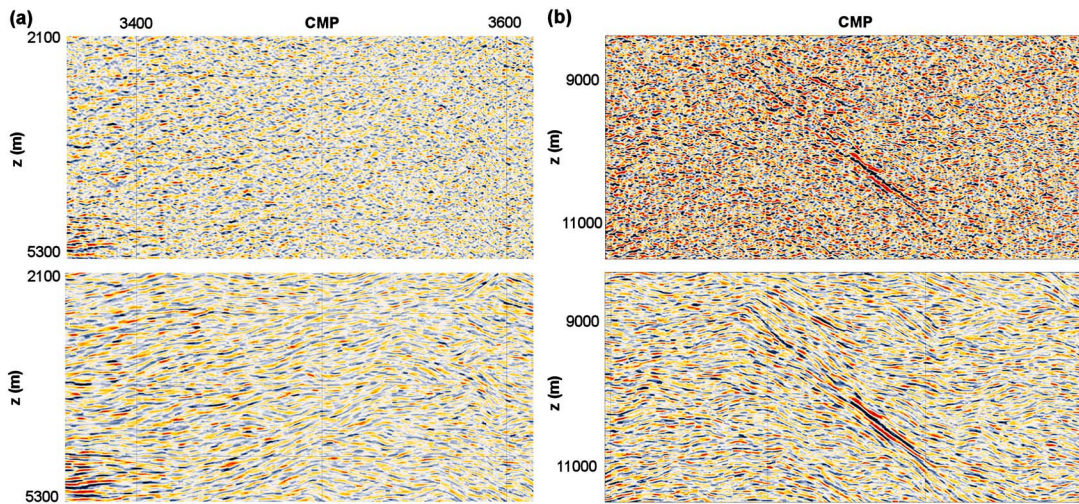
Figure 5. Examples illustrating the effects of the filtering at different scales and depths, with the original amplitude data (above) and the filtered data (below). No vertical exaggeration (scale 1:1). (a) A detail from close to the surface to the depth of 5000 m. Note the convergent reflection patterns in the centre of the filtered image (an example of the seismic facies SF2; see text and Figure 7). (b) A close-up from a depth of c. 8800–11,200 m. The results remain of equally high quality down to the depth of at least 15,000 m, to which this study was extended.

5. Observations from the Seismic Data

[16] The filtering reveals systematic packages of continuous reflections throughout the filtered section. The reflections were picked to produce a detailed line drawing of the structural trends in the southern part of FIRE 2A, to the depth of 15 km (Figure 6). Six distinct seismic facies were identified (Figure 7).

that the seismic facies approach described in the following chapter should be used in interpretation in order to enhance recognition of various structures and to reduce problems associated with 2D seismic data (see chapter 7.1).

Seismic facies refers to an assemblage of reflections with characteristic seismic parameters (e.g., energy, continuity, dip) and geometrical configurations [e.g., *Mitchum and Vail*, 1977]. Seismic facies result from geological features that are expressed as physical changes in the rock, such as anisotropy and lithological changes.

[17] The seismic facies 1 (SF1) consists of sigmoidal reflections that terminate onto moderately dipping, usually non-reflective zones. SF1 forms the background facies (the structural grain) of the interpreted section. The reflections of the seismic facies 2 (SF2) are usually somewhat bent to form sigmoidal reflections, but unlike in SF1, the reflections
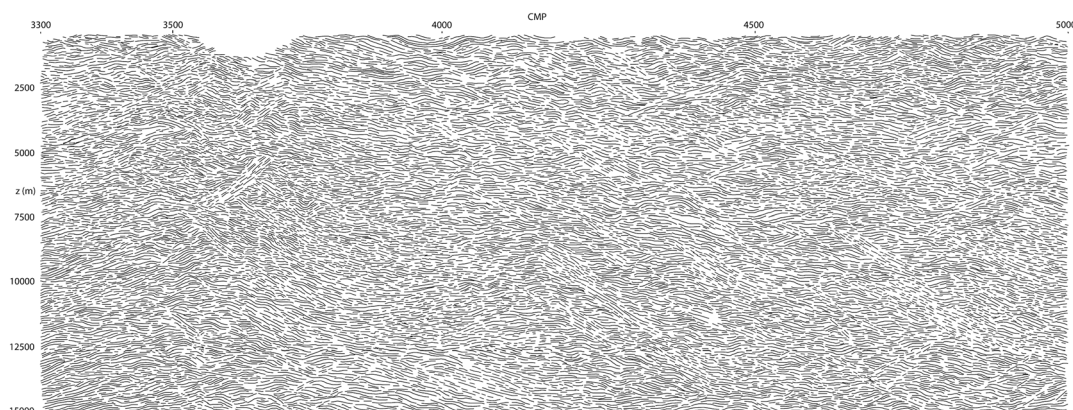

Figure 6. (a) Line drawing of the filtered seismic data. The line drawing was made by tracing the reflections revealed by the filtering. Various seismic facies were identified from the drawing in order to facilitate structural interpretation of the data (Figure 7).
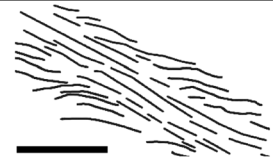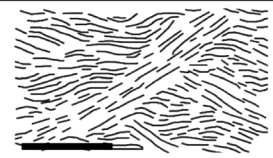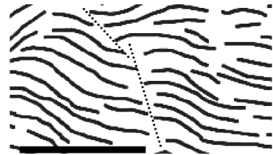
Seismic facies class		Description	Interpretation
SF1		Subhorizontal, sigmoidal reflections with terminations aligned into moderately dipping, relatively straight, non-reflective or weakly reflective zones	*Main S-C' facies:* S-C' structure, with the wavy reflections defining the C'-planes and the non-reflective / weakly reflective zones (and sometimes SF3) representing S-planes
SF2		Sets of converging reflections, often separated by straight, moderately dipping reflections	*Fold facies:* recumbent, isoclinals folds bounded by extensional/transtensional shear zones (i.e. the folds are affected by the S-C' folding and shearing)
SF3		Straight, moderately dipping reflections, flanked by reflections (of SF1/SF2) bent into (sub)parallelism with the straight reflections	*Shear zone facies:* Extensional / transtensional shear zone; some of these show higher energies (amplitudes) than others and may contain dykes. Often form an inherent part of the S-C' structures.
SF4		Various reflection types terminating along a non-reflective or weakly reflective, subhorizontal zone (marked with a stippled line)	*Detachment facies:* A subhorizontal detachment accommodating some of the overall extensional/ transtensional strain
SF5		Reflection assemblages showing characteristics of two or more of the other classes	*Complex facies:* interpretations vary
SF6		Reflections within SF1-SF5 terminating abruptly onto steeply dipping/subvertical, non-reflective planes (marked with stippled lines)	*Fault facies:* late, brittle faults cutting the ductile structures

Figure 7. Various seismic facies identified in the filtered FIRE2A seismic data. The scale is 1:1, the black scale bar is c. 1 km.

form converging sets. Both the SF1 and SF2 are commonly cut and/or overprinted by the seismic facies 3 (SF3). The SF3 is characterized by moderately dipping (apparent dip 20–50°), relatively straight reflections. The SF1 and SF2 reflections are bent into (sub)parallelism with the SF3 reflections. The facies SF1–SF3 show reflection terminations onto the subhorizontal, relatively straight, mostly unreflective features of the seismic facies 4 (SF4). The individual SF4 can be followed horizontally to up to 7 km along the interpreted section. The SF1–SF4 locally overlap, showing transitional and/or combined features (seismic facies 5, SF5). Seismic facies 6 (SF6) is characterized by disruptions marked by non-reflective and non-penetrative, sometimes branching, steeply dipping to subvertical planes. Unlike in the other facies, the terminations are not associated with bending of the reflections. The SF6 planes locally mark subtle offsets between horizons (at the limit of the seismic resolution). The SF6 overprints the whole studied interval and all the other seismic facies.

6. The Mode of the Mid-crustal Syn-orogenic Deformation

[18] The seismic facies observed in the data are interpreted to represent various deformation fabrics within the crust. The oldest identifiable structures are interpreted to be recumbent, tight to isoclinals folds, defined by the converging sub-horizontal reflections of SF2 (Figures 5a, 7, and 8). The imaging of the folds is facilitated by the fact that the seismic profile is perpendicular to the trend of the axial planes (Figure 2). The geological maps and previous studies illustrate complex fold interference patterns originating from the crustal thickening phase(s) of the orogeny [e.g., *Schreurs and Westra*, 1986]. The fold interference resulted mostly
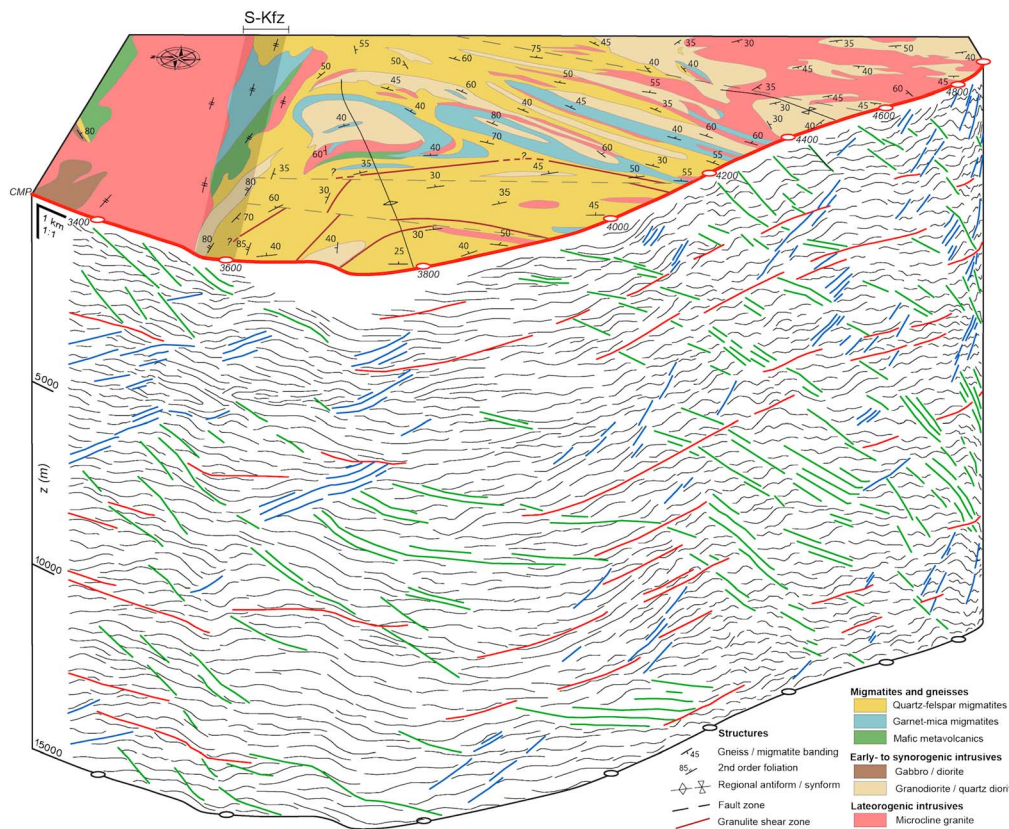
Figure 8. Block diagram illustrating the interpretation of the seismic data combined with the surface geological map and structural observations. The intensely sheared granulite zones (Figure 3c), offset by late, dominantly brittle fault zones, are marked on the geological map with reddish-brown lines. In the seismic reflection data interpretation, colors are used to emphasize the various geometries, i.e., the shear zones (blue and green) and the subhorizontal detachments (red). Some recumbent, isoclinals folds are also interpreted in the seismic data. The "2nd order foliation" refers to foliations overprinting the migmatitic and gneissose banding, i.e., younger deformation. In the field, the Somero-Karkkila fault zone (S-Kfz) displays significant regional (along-strike) overprinting of the granulite-facies features by post-migmatitic shearing with retrograde, lower amphibolite to greenschist facies metamorphism and semi-brittle faulting. The brittle fault interpretations are omitted from the seismic line drawing for clarity. See text for further discussion.

in recumbent, tight to isoclinal fold patterns with moderately to gently dipping hinge lines and axial planes, forming the gently dipping to subhorizontal structural layering within West Uusimaa [*Skyttä and Mänttäri*, 2008]. It is, therefore, suggested that the SF2 records the thickening phase of the Svecobaltic orogeny.

[19] The recumbent fold facies of SF2 is deformed by SF1 and SF3. The SF1 is present throughout the interpreted section (Figures 6 and 8). Together with the more local SF3, the SF1 forms kilometer-scale S-C′ structures that geometrically indicate extension (Figures 8 and 9; the first-order orogen-scale shear plane is assumed to be subhorizontal, to distinguish between S-C and S-C′ structures; for more detailed information about the kinematic significance of S-C′ geometries, see, e.g., *Lister and Snoke*, 1984]. The S-C′ structures accommodate the lateral extension of the orogen, both toward the SE and NE

(apparent direction along the 2D profile; Figure 8). The moderately dipping SF3 are, therefore, interpreted as extensional/transtensional shear zones forming an inherent part of the mega-scale S-C′ system (Figures 7 and 8).

[20] The subhorizontal features of SF4 are interpreted as detachment surfaces, accommodating significant part of the extensional strain (Figure 9). They are unlikely to be artifacts: the SF4 are not the dominant reflections and are systematically marked by reflection terminations of the other seismic facies. The SF4 detachments are several kilometers long and bound several SF1–SF3 assemblages, but they are not continuous through the WUC. The characteristic vertical spacing between the detachments is in the order of 1–2 km.

[21] Reflection assemblages falling into SF5 (complex facies) are usually spatially associated with the
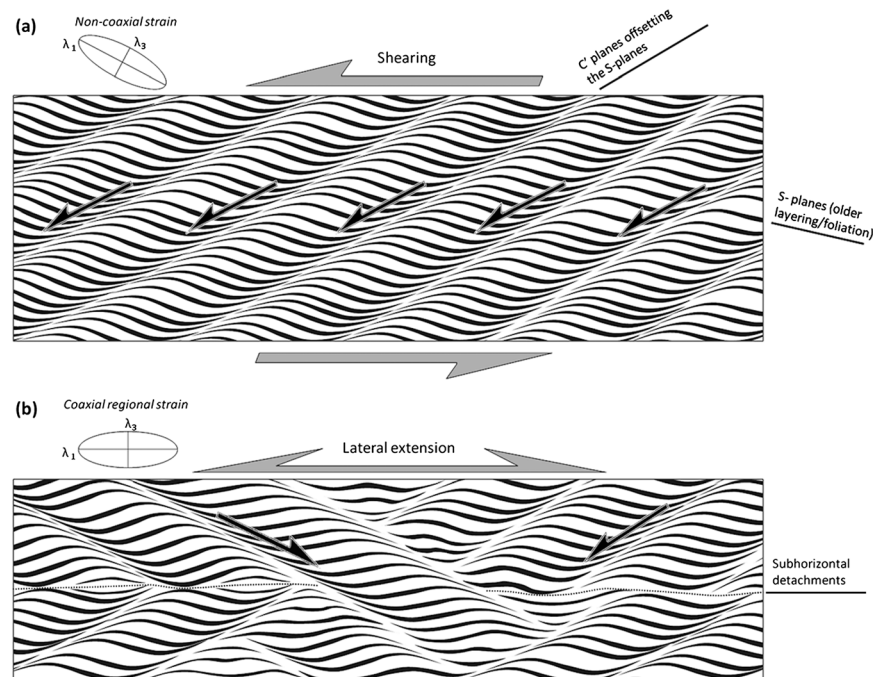
Figure 9. Schematic drawings of the structural geometries discussed in the text. In the strain ellipses, $\lambda_1 =$ approximate maximum extension (stretching), $\lambda_3 =$ approximate minimum extension or maximum shortening. (a) The principle of the kinematics forming S-C′ structural geometries. In shear zones with non-coaxial strain, S-C′ structures ideally develop onto pre-existing layering (foliation) forming symmetric sigmoidal patterns, as illustrated here. (b) The S-C′ patterns formed as a result of coaxial strain and lateral escape in 2D. The lateral escape of the material (i.e., extension) at a large scale is accommodated by the "doubly-vergent" S-C′ structures. Where the S-C′ patterns with opposing vergences meet, subhorizontal weakness zones develop ("detachments"; stippled lines). The pattern illustrated here is the same as revealed by the filtered seismic data; the doubly-vergent mega-scale S-C′ structures accommodate the crustal extension within the WUC.

steeply dipping Somero-Karkkila fault zone (S-Kfz; Figures 2 and 8). The complexity of structures is interpreted to at least partly result from a significant strike-slip component along the S-Kfz (out-of-plane with respect to the seismic section). At least some of the strike-slip movements post-date the extension and the observable surface features along the S-Kfz are dominated by the second-order foliations (Figure 8). However, the aeromagnetic and the field data suggest the presence of an earlier significant geological boundary or shear zone, possibly a terrane boundary (Figure 2). The early boundary was obscured by the extension, which may in part have contributed to the complex seismic facies in this area. Either way, the NMO migration does not allow detection of reflections much steeper than c. 40° (Figures 4b and c).

[22] The subvertical planes of SF6 that disrupt the observed seismic facies are interpreted as steeply dipping fault and fracture zones, some of which are associated with the late movements along the S-Kfz. Field observations indicate that they are late, brittle-ductile to brittle features cross-cutting the

ductile structures. The post-orogenic history of the WUC is not the focus of this study, so the late faults will not be discussed further.

[23] The strain type (plane strain vs. general strain) plays a role in the final structural geometries. A "2D" plane strain would be expected to produce a set of conjugate shear zones with opposite dips. In the case of non-plane, i.e., general strain, five slip planes are theoretically required to accommodate the strain in three dimensions. In a 2D (seismic) profile, only two or three of these would, however, be seen. The variable dip directions of the reflections (Figure 4b) imply that the strain type in the study area is general strain. However, the dominant extension/flow direction cannot be deduced from the available seismic data. A correlation of the seismic data with the exposed surface geology helps in the interpretation of the 3D geometry of the reflections (Figures 4 and 8). In places, the S-C′ facies (SF1) and the associated shear zones (SF3) can be correlated with kilometer-scale gentle folds. An open synform, observed between CMPs 4400 and 4600 in the field (Figure 8), is interpreted as the

surface expression of the combination of the SF1 sinuous reflections and the SF3 shear zones with opposing dips, seen in the seismic data. The antiformal structure around CMP 3800 is similarly expressed by the combination of the SF1 and SF3. The felsic pyroxene-bearing granulite shear zones observed at outcrop, such as shown in Figure 3c, correlate with shear zones interpreted in seismic (e.g., the shear zone at CMP c. 3910 in Figure 8). It should be noted that due to locally poor exposure, there may be many more of such shear zones than those shown in the geological map of Figure 8 (e.g., around CMP4200–4250). Inversely, missing seismic data just south of the S-Kfz (due to the presence of the town of Karkkila) prevent reliable correlation between outcrop and subsurface structures. The same is true for areas that are covered by the late-orogenic granite laccoliths. With respect to the third dimension of the general strain, both the antiformal structure around CMP 3800 and the granulite shear zones are partly eastward dipping, implying a significant orogen-parallel extensional/flow component. A more quantitative estimation of the amount of orogen-perpendicular vs. orogen-parallel flow is a scope for future work.

7. Discussion

7.1. Problems with Filtering and Interpreting 2D Data

[24] The 2D nature of most seismic reflection data acquired from the crystalline basement, together with the often complicated geological history and the resulting heterogeneity at various scales, creates some issues that need to be borne in mind when filtering and interpreting the data. The crustal heterogeneities and the often complex geometries cause reflection patterns that can be difficult to interpret. The crustal heterogeneity can also lead to significant scattering of the seismic signal, especially at greater depths, while processing and imaging techniques frequently assume weak/single scattering and uniform transmission throughout the crust [e. g., *Wu and Aki*, 1988; *Levander et al.*, 1994]. As greater depths are approached (>4 seconds two-way-time), strong and multiple scattering progressively degrade the signal. The FIRE seismic data presented here is filtered and interpreted down to 15 km depth (<5 s TWT). The imaged section between 0 and 15 km lies mostly in the optical regime (Figure 4a) where conventional migration based on ray theory can be expected to work reasonably well [*Wu and Aki*, 1988].

[25] A well-known issue with 2D seismic reflection data is the so-called out-of-plane reflections ("side-swipe"). The input from out-of-plane reflections increases systematically toward greater depths, progressively producing a mixture of in-plane and out-of-plane reflections. To decrease this problem, a seismic profile should be shot at right angles to the structural (geological) strike, and the more the profile diverges from this geometry, the more likely it is to contain out-of-plane reflections. In reality, small variations occur both in the geological strike and in the strike of the seismic profile, resulting in out-of-plane reflections [e.g., *Drummond et al.*, 2004]. Strong out-of-plane reflectors typically produce reflections in the migrated profile that cross-cut the in-plane reflections. The out-of-plane reflections do not seem to be a significant problem in the filtered FIRE data (Appendix III). The profile in the studied area is for most parts at right angles to the strike. Artifacts such as cross-cutting or "bow-tie" reflections were not encountered during picking of the filtered data. The interpretation technique used in this paper, based on the seismic facies concept, also reduces the risk of incorporating occasional out-of-plane reflections into the interpretation; the concept is based on the consideration of the general reflection patterns and packages, rather than individual reflections. Therefore, it separates the different 2D architectures reflecting the relative 3D heterogeneities between units. Finally, the structural pattern (the S-C′ structures) is not only observed close to the surface where out-of-plane reflections are less likely to interfere, but also at greater depths, indicating that the interpretation of the overall structural pattern is valid to the depth of 15 km.

7.2. The Seismic Reflection Patterns within the Orogenic Crust, and the Mode of Extension/Lateral Flow

[26] The extensional architecture dominates the interpreted FIRE seismic data from the middle and lower orogenic crust, currently exposed at the Earth surface. The apparent extensional geometries need not, however, imply an extensional overall tectonic setting or thinning of the lithosphere. The crust in southern Finland is still 45–50 km thick, after at least 15 km of erosion [*Grad et al.*, 2009]. Several landmark studies have established the importance of syn- to late-convergent "extensional" and flow processes: continental plateau development and crustal coupling-decoupling [e.g., *Kellett and Grujic*, 2012; *Sokoutis and Willingshofer*, 2011], orogenic collapse [e.g., *Dewey*, 1988; *Rey et al.*,

2001], and mid-crustal flow [e.g., *Beaumont et al.*, 2001; *Grujic et al.*, 2011; *Culshaw et al.*, 2006; *Vanderhaege and Teyssier*, 2001]. To which orogenic process the S-C′ structures in the WUC belong to is beyond the scope of this study. The age determinations from the WUC anatectic granites, however, imply that the processes that formed the S-C′ structures were (early) synorogenic with respect to the c. 1.85–1.82 Ga Svecobaltic orogen [e.g., *Kurhila et al.*, 2005; *Skyttä and Mänttäri*, 2008]. Therefore, it may be feasible to preliminarily speculate that the structures were formed as a result of syn-orogenic mid-crustal flow rather than late-orogenic collapse. The original subhorizontal to gently dipping foliations and other structures (including the recumbent folds) formed during the thickening phase of the Svecobaltic orogeny [*Lahtinen et al.*, 2005; *Skyttä and Mänttäri*, 2008], and were subsequently extended by the mid-crustal flow. This scenario implies that the gently to moderately dipping shear zones along with the rest of the S-C′ structures would, therefore, have formed at this stage, i.e., at c. 1.84–1.80 Ga ago. Dating of the granulite shear zones is in process, and the results are expected to provide more information on the timing of the extension. The published P-T-time paths for southern Finland [e.g., *Cagnard et al.*, 2007; *Väisänen and Hölttä*, 1999] and the present erosion level at which pervasive migmatization and, therefore, weakening of the crust occurred correspond well to the mid-crustal flow models presented in the literature [e.g., *Beaumont et al.*, 2001] although they are not exclusive to mid-crustal flow. On the other hand, the interpreted palaeodepth of c. 15 km is shallower than the suggested depth of mid-crustal flow in the Himalayas [from c. 30 km downwards; e.g., *Grujic et al.*, 2011]. If the structures in the FIRE profiles resulted from mid-crustal flow, implications for the geothermal gradient in the Palaeoproterozoic time may be significant.

[27] The strain distribution is more penetrative and smaller-scale than implied by the preliminary FIRE 2A interpretation [*Nironen et al.*, 2006]. The pervasive nature of the deformation is expressed by the interference between the various structures. The early recumbent folds, formed during orogenic thickening, are deformed by the S-C′ structures. The structures interact with each other: the crustal shear zones (SF3) are not continuous, but strain transfer occurs both via distributed deformation (SF1) and along subhorizontal planes (SF4; Figures 8 and 9). Our results support recent models of crustal-scale strain transfer along both dipping and subhorizontal shear

zones in extending/flowing orogenic crust [*Chardon et al.*, 2011; *Wang et al.*, 2011]. Specifically, *Chardon et al.* [2011] suggest that, based on their field studies, the crustal extension in the Dharwar craton (southern India) was accommodated by a network of structures that very much resembles the kilometer-scale S-C′ structures presented in this study. A somewhat contrasting view is taken by *Regenauer-Lieb et al.* [2008], who show that, based on numerical modelling, the strain in an extending lithospheric crust should partition into distinct, conjugate sets of extensional shear zones. However, an extensional tectonic setting and lithospheric thinning is not necessary for orogenic mid-crustal flow or orogenic collapse. It is true that a significant amount of the strain is accommodated by the shear zones in the WUC (SF3), but much of the strain is also taken up by the volumes between the shear zones (SF1) and the subhorizontal detachments (SF4), so that the overall pattern rather resembles a three-dimensional network than a set of conjugate shear zones (which is a natural consequence of general strain). The absence of a distinct pressure or temperature jump in and in the vicinity of the WUC can, therefore, be explained by the S-C′ structures: this mode of orogenic extension allows the accommodation of large regional strains without the need to develop crustal-scale detachment zones.

[28] A two to three orders of magnitude decrease in the overall rock strength, compared to unmolten rock (0% melt), is achieved with a few percents of melt within the rock volume [e.g., *van der Molen and Paterson*, 1979; *Vanderhaege*, 2009]. The most significant drop in the rheological strength occurs at a melt fraction of c. 0.07 [*Rosenberg and Handy*, 2005]. Importantly, at these low melt percentages, the rock can still deform as a solid, granular mass, meaning that strains can be taken up by the entire volume rather than just by the melt-bearing zones. The mechanical transition from solid to liquid occurs at about 30–40% melt fraction [e.g., *Rutter and Neumann*, 1995; *van der Molen and Paterson*, 1979], although even lower percentages of $20 \pm 10\%$ have been suggested by *Arzi* [1978]. A low amount of melts in the crust is important for the formation of the S-C′ pattern, as the crust needs to flow but simultaneously behave and deform as a solid mass rather than as a liquid. On the other hand, crustal deformation enhances melt migration and accumulation at certain crustal levels [e.g., *Vanderhaege*, 2009]. High melt percentages and melt accumulation result in strong strain partitioning [e.g., *Holtzman et al.*, 2003; *Vanderhaege*, 2009]. In the study area, field data imply that some of the melts were removed from

the deeper crust and accumulated into larger melt pockets within the crust (e.g., the c. 1.83 Ga microcline granite laccoliths at the present erosion level). However, the laccoliths themselves are not deformed to the extent to suggest strong strain partitioning, which implies that they did not accommodate the bulk of the strain. The melt transport might have been largely syn-deformational, but the final accumulation of the melts seems to have occurred later. As the melt accumulations grew the strain may, however, have progressively partitioned into the melt layers. Therefore, a temporal evolution of the strain partitioning is implied.

[29] The physical properties of the rock, such as lithological changes and mineral anisotropy, influence the obtained seismic reflectivity [e.g., *Lloyd et al.*, 2009]. The unfiltered FIRE2A seismic data show few prominent reflective areas, while most of the interpreted section is non-reflective and noisy (e.g., Figure 5a). Therefore, it is unlikely that large, systematic lithological contrasts (suitable for generating significant acoustic impedance contrasts) exist in the crust within the interpreted section. However, the filtering reveals a penetrative fabric throughout the seismic section, even in the "white," noisy areas (Figure 5). It has been demonstrated elsewhere that the seismic anisotropy, one mechanism for generating reflections from the crust in the seismic data, results from rock fabrics (i.e., deformation) rather than lithological layering [e.g., *Weiss et al.*, 1999]. More specifically, the seismic anisotropy is usually attributed to the presence of regionally aligned mica and, in the lower crust, amphibole [e.g., *Lloyd et al.*, 2009; *Shapiro et al.*, 2004; *Tatham et al.*, 2008]. Both aligned mica and amphiboles/pyroxenes are abundant in the studied area, and they follow and define the fabrics of the rocks. The structures observed at outcrop are generally gently to moderately dipping, which explains their efficient imaging at depth by the seismic data. Therefore, the observed seismic reflection patterns, revealed by the filtering, are here attributed to the internal mineral anisotropy, i.e., the structural fabric of the rocks, rather than lithological variation at the scale of the reflections.

7.3. Implications to Interpretation of Crustal Seismic Data

[30] Acoustic boundaries in the deep crust are usually due to lithological changes, and do not always correspond to structural boundaries. Structural interpretation of seismic reflection data should not, therefore, rely solely on the examination of (wiggle) amplitude images. Furthermore, distinguishing extensional structures (local or crustal-scale) from compressional ones can be difficult even when the exposures can be observed directly in three dimensions (*Butler and Freeman*, 1996; *Wheeler and Butler*, 1994). The significant uncertainties related to structural interpretation of seismic reflection data from the crystalline basement can be reduced by advanced seismic attribute analysis: the dip-steering median filter allows a more reliable and detailed detection of the deformation structures within the crust.

[31] In the studied seismic section, many seismic features in the mid-crust might generally be attributed to crustal thickening and/or thrusting. Fold structures mapped in the field are also commonly attributed to contractional deformation. However, after an examination of the seismic attributes and the structural trends, the reflections in the FIRE2A seismic data and the kilometer-scale gentle folds observable in the field are more plausibly interpreted to result from pervasive crustal extension. The extensional features overprint and obscure most of the earlier structures in the seismic data, including the terrane boundary (S-Kfz), although some of the extensional structures may follow and invert earlier (thrust) structures. This observation conforms to some previous works suggesting that the seismic fabrics from orogenic belts reflect the pervasive structural overprinting due to late orogenic processes [e.g., *Oncken*, 1998]. The mode of the structural overprinting in hot orogenic roots is, however, extensional rather than compressional, resulting from syn-orogenic mid-crustal flow and/or syn- to late-orogenic collapse. It should be repeated, however, that this does not imply overall extensional tectonic setting and lithospheric thinning, e.g., *Beaumont et al.*, 2001; *Grujic et al.*, 2011).

[32] Modern seismic attribute methods should be utilized in and developed for crystalline basement studies, in order to facilitate increasingly detailed structural interpretation of crustal seismic datasets. However, the limitations caused by 2D data and the crustal heterogeneities have to be considered because the reliability of filtering techniques decreases at great depths. Therefore, the seismic facies interpretational approach should be utilized in interpreting filtered seismic data. The seismic attribute method described in this paper should be applicable to other deep seismic datasets, possibly even vintage data [e.g., INDEPTH, NFP20, LITHOPROBE; e.g., *Choukroune and ECORS Team*, 1989; *Clowes et al.*, 1992; *Klemperer and Hobbs*, 1991; *Nelson et al.*, 1996). The method can be utilized to study the mode and the geometries of sub-kilometer-scale, gently to moderately dipping structural fabrics of the last penetrative deformation phase in the studied dataset. The last penetrative deformation phase is recorded as patterns of reflections (seismic facies). Systematic discontinuities of the reflections, marking

later (steep) fault zones and fractures, may also be more reliably detectable in filtered data. Further developments in the calibration of complex attribute methods to suit crustal studies could also permit (semi-) quantitative approaches to the geological processes within the crust.

8. Conclusions

[33] This study shows that the seismic reflection data from the crystalline basement, even after initial processing, can be significantly enhanced by seismic attribute analysis. A filtering technique, based on the dip attribute, is described and applied to processed seismic data from Palaeoproterozoic, exposed orogenic roots. The filtered data are interpreted using the seismic facies approach. The filtering and the interpretation reveal detailed, sub-kilometer-scale penetrative deformation fabrics within the extended middle and lower crust: the extensional strain is accommodated by mega-scale S-C′ structures overprinting earlier structures in the seismic data. The seismic data, therefore, record the last phase of penetrative ductile deformation within the middle and lower crust.

[34] Modern seismic attribute techniques can be used with care to enhance imaging of other seismic reflection datasets from crystalline basement. The method described in this paper is potentially applicable to vintage datasets as well as to modern seismic data. The application of modern seismic attribute approaches in general to seismic reflection data from crystalline basement should be further developed: by using seismic attributes, combined with interpretation based on the seismic facies concept, more detailed, sub-kilometer-scale structural information can be extracted from the data, while the interpretational uncertainty is reduced.

Acknowledgments

[36] OpendTect workflow documentations can be found at: http://www.opendtect.org/rel/doc/User/workflows/. For a detailed description of the dip-steering plugin, see http://opendtect.org/rel/doc/User/dgb/ (chapters 2 and 10.2).

References

Arzi, A. A. (1978), Critical phenomena in the rheology of partially melted rocks, *Tectonophysics*, *44*, 173–184.

Barnes, A. E. (2001), Seismic attributes in your facies, *CSEG Recorder*, *26*, 41–47.

Beaumont, C., R. A. Jamieson, M. H. Nguyen, and B. Lee, (2001) Himalayan tectonics explained by extrusion of a low-viscosity crustal channel coupled to focused surface denudation, *Nature*, *414*, 738.

Brouwer, F., and A. Huck (2011). An integrated workflow to optimize discontinuity attributes for the imaging of faults, in 2011 Proceedings: Attributes: New Views on Seismic Imaging—Their Use in Exploration and Production, edited by K. J. Marfurt, D. Gao, A. Barnes, S. Chopra, A. Corrao, B. Hart, H. James, J. Pacht, and N. C. Rosen, pp. 496–533, *GCSSEPM, 31st Annual Conference publication*.

Butler, R. W. H., and S. Freeman (1996), Can crustal extension be distinguished from thrusting in the internal parts of mountain belts? A case history of the Entrelor shear zone, Western Alps, *J. Struct. Geol.*, *18*, 909–923.

Cagnard, F., D. Gapais, and P. Barbey (2007), Collision tectonics involving juvenile crust: The example of the southern Finnish Svecofennides, *Precambrian Res.*, *154*, 125–141.

Chardon, D., M. Jayananda, and J.-J. Peucat (2011), Lateral constrictional flow of hot orogenic crust: Insights from the Neoarchaean of south India, geological and geophysical implications for orogenic plateaux, *Geochem. Geophys. Geosyst.*, *12*, doi:10.1029/2010GC003398.

Choukroune, P., and ECORS Team (1989), The Ecors Pyrenean deep seismic profile reflection data and the overall structure of an orogenic belt, *Tectonics*, *8*, 23–39.

Clowes, R. M., F. A. Cook, A. G. Green, C. E. Keen, J. N. Ludden, J. A. Percival, G. M. Quinlan, and G. F. West (1992), Lithoprobe: New perspectives on crustal evolution, *Can. J. Earth Sci.*, *29*, 1813–1864.

Coney, P. J., and T. A. Harms (1984), Cordilleran metamorphic core complexes: Cenozoic extensional relics of Mesozoic compression, *Geology*, *12*, 550–554.

Culshaw, N. G., C. Beaumont, and R. A. Jamieson (2006). The orogenic superstructure-infrastructure concept: Revisited, quantified, and revived, *Geology*, *34*, 733–736.

Dewey, J. F. (1988), Extensional collapse of orogens, *Tectonics*, *7*, 1123–1139.

Drummond, B. J., T. J. Barton, R. J. Korsch, N. Rawlinson, A. N. Yeates, C. D. N. Collins, and A. V. Brown (2000), Evidence for crustal extension and inversion in eastern Tasmania, Australia, during the Neoproterozoic and Early Palaeozoic. *Tectonophysics*, *329*, 1–21.

Drummond, B. J., R. W. Hobbs, and B. R. Goleby (2004), The effects of out-of-plane seismic energy on reflections in crustal-scale seismic sections, *Tectonophysics*, *388*, 213–224.

Eaton, D. W. S., and F. A. Cook (1988), LITHOPROBE seismic reflection imaging of Rocky Mountain structures east of Canal Flats, British Columbia, *Can. J. Earth Sci.*, *25*, 1339–1348.

Ehlers, C., A. Lindroos, and O. Selonen (1993), The late Svecofennian granite–migmatite zone of southern Finland—

a belt of transpressive deformation and granite emplacement, *Precambrian Res.*, *64*, 295–309.

Eskola, P. (1915), On the relation between the chemical and mineralogical composition in the metamorphic rocks of the Orijärvi region. *Bull. Comm. Géol. Finlande 44*.

Fernández-Viejo, G., J. Gallastegui, J. A. Pulgar, and J. Gallart (2011), The MARCONI reflection seismic data: A view into the eastern part of the Bay of Biscay, *Tectonophysics*, *508*, 34–41.

Fertig, J., M. Thomas, and R. Thomas (1999), How to remedy non-optimal seismic data by seismic processing, *Pure Appl Geophys*, *156*, 345–370.

Gaál, G., and R. Gorbatschev (1987), An outline of the Precambrian evolution of the Baltic Shield, *Prec. Res.*, *35*, 15–52.

Grad, M., T. Tiira, and ESC Working Group (2009), The Moho depth map of the European Plate, *Geophys. J. Int.*, *176*, 279–292.

Grad, M., and U. Luosto (1987), Seismic models of the crust of the Baltic Shield along the SVEKA profile in Finland, *Ann. Geophys.*, *5B*(6), 639–650.

Grujic, D., C. J. Warren, and J. Wooden (2011), Rapid syn-convergent exhumation of Miocene-aged lower orogenic crust in the Eastern Himalaya, *Lithosphere*, *3*, 346–366.

Holliger, K., A. Levander, R. Carbonell, and R. Hobbs (1994), Some attributes of wavefields scattered from Ivrea-type lower crust, *Tectonophysics*, *232*, 267–279.

Holtzman, B. K., D. L. Kohlstedt, M. E. Zimmermann, F. Heidelbach, T. Hiraga, and J. Hustoft (2003), Melt segregation and strain partitioning: Implications for seismic anisotropy and mantle flow, *Science*, *301*, 1227–1230.

Iacopini, D., and R. W. H. Butler (2011), Imaging deformation in submarine thrust belts using seismic attributes, *Earth Planet. Sci. Lett.*, *302*, 414–422.

Kellett, D., and D. Grujic (2012), New insight into the South Tibetan detachment system: Not a single progressive deformation, *Tectonics*, *31*, doi:10.1029/2011TC002957.

Klemperer, S. L., and R. Hobbs (1991), The BIRPS Atlas: Deep Seismic Reflection Profiles Around the British Isles, Cambridge University Press, p. 117.

Korja, A., and P. J. Heikkinen (1995), Proterozoic extensional tectonics of the central Fennoscandian Shield: Results from the Baltic and Bothnian Echoes from the Lithosphere experiment. *Tectonics*, *14*, 504–517.

Korsman, K., T. Koistinen, J. Kohonen, M. Wennerström, E. Ekdahl, M. Honkamo, H. Idman, and Y. Pekkala (Eds.) (1997), Bedrock Map of Finland 1:1000000, *Geol. Survey of Finland*.

Kukkonen, I. T., P. Heikkinen, E. Ekdahl, S.-E. Hjelt, J. Yliniemi, E. Jalkanen, and FIRE Working Group (2006), Acquisition and geophysical characteristics of reflection seismic data on FIRE transects, Fennoscandian Shield, *Geol. Survey of Finland Spec. Paper*, *43*, 13–43.

Kurhila, M., I. Mänttäri, M. Vaasjoki, O. T. Rämö, and M. Nironen (2011), U-Pb geochronological constraints of the late Svecofennian leucogranites of southern Finland, *Precambrian Res.*, *190*, 1–24.

Kurhila, M., M. Vaasjoki, I. Mänttäri, T. Rämö, and M. Nironen (2005), U-Pb ages and Nd isotope characteristics of the lateorogenic, migmatizing microcline granites in southwestern Finland, *Bull. Geol. Soc. Finland*, *77*, 105–128.

Lahtinen, R., A. Korja, and M. Nironen (2005), Palaeoproterozoic tectonic evolution, in Precambrian Geology of Finland – Key to the Evolution of the Fennoscandian Shield, edited by M. Lehtinen, P. A. Nurmi, O. T. Rämö, pp. 481–532, Elsevier B V, Amsterdam.

Levander, A., R. W. Hobbs, S. K. Smith, R. W. England, D. B. Snyder, and K. Holliger (1994), The crust as a heterogeneous "optical" medium, or "crocodiles in the mist", *Tectonophysics*, *232*, 281–297.

Lister, G. S., and A. W. Snoke (1984), S-C mylonites, *J. Struct. Geol.*, *6*, 617–638.

Lloyd, G. E., R. W. H. Butler, M. Casey, and D. Mainprice (2009), Mica, deformation fabrics and the seismic properties of the continental crust, *Earth Planet. Sci. Lett.*, *288*, 320–328.

Meissner, R., and R. K. Bortfeld (1990), DEKORP Atlas: Results of Deutsches Kontinentales Reflexionsseismisches Programme, 311 pp., Springer-Verlag.

Mitchum, R. M., and P. R. Vail (1977), Seismic stratigraphic interpretation procedure, in Seismic Stratigraphy—applications to hydrocarbon exploration, AAPG Memoir, Vol. *26*, Edited by C. E. Payton, p. 516.

Mouri, H., M. Väisänen, H. Huhma, and K. Korsman (2005), Sm-Nd garnet and U-Pb monazite dating of high-grade metamorphism and crustal melting in the West Uusimaa area, southern Finland, *GFF 127*, 123–128.

Nelson, K. D., et al. (1996), Partially molten middle crust beneath southern Tibet: Synthesis of Project INDEPTH results, *Science*, *274*, 1684–1688.

Nironen, M., A. Korja, P. Heikkinen, and the FIRE Working Group (2006), A geological interpretation of the upper crust along FIRE 2 and FIRE 2A. *Geol. Survey of Finland Spec. Paper*, *43*, 77–103.

Oncken, O. (1998), Orogenic mass transfer and reflection seismic patterns—evidence from DEKORP sections across the European Variscides (central Germany), *Tectonophysics*, *286*, 47–61.

Pajunen, M., M.-L. Airo, T. Elminen, I. Mänttäri, R. Niemelä, M. Vaarma, P. Wasenius, and M. Wennerström (2008), Tectonic evolution of the Svecofennian crust in southern Finland, *Geol. Survey of Finland Spec. Paper*, *47*, 15–160.

Randen, T., and L. Sønneland (2005), Mathematical methods and modelling, in *Hydrocarbon Exploration and Production*, *Mathematics in Industry*, Vol. 7, Edited by A. Iske, and T. Randen, Springer, Berlin, Heidelberg.

Regenauer-Lieb, K., G. Rosenbaum, and R. F. Weinberg (2008). Strain localisation and weakening of the lithosphere during extension. *Tectonophysics*, *458*, 96–104.

Rey, P. F. (1993), Seismic and tectono-metamorphic characters of the lower continental crust in Phanerozoic areas: A consequence of post-thickening extension, *Tectonics*, *12*, 580–590.

Rey, P., O. Vanderhaege, and Teyssier C. (2001). Gravitational collapse of the continental crust: Definition, regimes and modes, *Tectonophysics*, *342*, 435–449.

Rey, P. F., C. Teyssier, and D. L. Whitney (2009), The role of partial melting and extensional strain rates in the development of metamorphic core complexes, *Tectonophysics*, *477*, 135–144.

Rosenberg, C. L., and M. R. Handy (2005), Experimental deformation of partially melted granite revisited: Implications for the continental crust, *J. Metam. Geol.*, *23*, 19–28.

Royden, L. H., B. C. Burchfiel, R. W. King, E. Wang, Z. Chen, F. Shen, and Y. Liu (1997), Surface deformation and lower crustal flow in eastern Tibet, *Science*, *276*, 788–790.

Rutland, R. W. R., I. S. Williams, and K. Korsman (2004), Pre-1.91 Ga deformation and metamorphism in the Palaeoproterozoic Vammala Migmatite Belt, southern Finland, and implications for Svecofennian tectonics, *Bull. Geol. Soc. Finland*, *76*, 93–140.

Rutter, E. H., J. Khazanehdari, K. H. Brodie, D. J. Blundell, and D. A. Waltham (1999), Synthetic seismic reflection profile through the Ivrea zone — Serie dei Laghi continental crustal section, northwestern Italy, *Geology*, *27*, 79–82.

Rutter, E. H., and D. H. K. Neumann (1995), Experimental deformation of partially molten Westerly granite under fluid-absent conditions, with implications for the extraction of granitic magmas, *J. Geophys. Res.*, *100*, 15697–15715.

Schreurs, J., and L. Westra (1986), The thermotectonic evolution of a Proterozoic, low pressure, granulite dome, West Uusimaa, SW Finland, *Contrib. Mineral. Petrol.*, *93*, 236–250.

Sederholm, J. J. (1926), On migmatites and associated pre-Cambrian rocks of southwestern Finland, part II. The region around Barösundsfjärd W of Helsingfors and neighbouring areas, *Bull. Comm. Géol. Finlande*, *77*, 143.

Shapiro, N. M., M. H. Ritzwoller, P. Molnar, and V. Levin (2004), Thinning and flow of Tibetan crust constrained by seismic anisotropy, *Science*, *305*, 233.

Skyttä, P., and I. Mänttäri (2008), Structural setting of late Svecofennian granites and pegmatites in Uusimaa Belt, SW Finland: Age constraints and implications for crustal evolution, *Precambrian Res.*, *164*, 86–109.

Sokoutis, D., and E. Willingshofer (2011). Decoupling during continental collision and intra-plate deformation, *Earth Planet. Sci. Lett.*, *305*, 435–444.

Stel, H., R. Veenhof, J. M. Huizenga, M. Timmermann, J. M. H. Hartsink (1989), Infra-supra structure relations of a microcline-granite dome in the Somero area, Svecofennides, SW Finland, *Bull. Geol. Soc. Finland*, *61*, 131–134.

Taner, M. T., F. Koehler, and R. E. Sheriff (1979), Complex seismic trace analysis, *Geophysics*, *44*, 1041–1063.

Taner, M. T. (2001), Seismic attributes, *CSEG Recorder*, *26*, 48–55.

Tatham, D. J., G. E. Lloyd, R. W. H. Butler, and M. Casey (2008), Amphibole and lower crustal seismic properties, *Earth Planet. Sci. Lett.*, *267*, 118–128.

Väisänen, M., and P. Hölttä (1999), Structural and metamorphic evolution of the Turku migmatite complex, southwestern Finland, *Bull. Geol. Soc. Finland*, *71*, 177–218.

Vanderhaege, O. (2009), Migmatites, granites and orogeny: Flow modes of partially-molten rocks and magmas associated with melt/solid segregation in orogenic belts, *Tectonophysics*, *477*, 119–134.

Vanderhaege, O., and C. Teyssier (2001), Partial melting and flow of orogens, *Tectonophysics*, *342*, 451–472.

Van der Molen, I., and M. S. Paterson (1979), Experimental deformation of partially-melted granite, *Contrib. Mineral. Petrol.*, *70*, 299–318.

Wang, C., R. Gao, A. Yin, H. Wang, Y. Zhang, T. Guo, Q. Li, and Y. Li (2011), A mid-crustal strain-transfer model for continental deformation: A new perspective from high-resolution deep seismic-reflection profiling across NE Tibet, *Earth Planet. Sci. Lett.*, *306*, 279–288.

Weiss, T., S. Siegesmund, W. Rabbel, T. Bohlen, and M. Pohl (1999), Seismic velocities and anisotropy of the lower continental crust: A review, *Pure Appl. Geophys.*, *156*, 97–122.

Wheeler, J., and R. W. H. Butler (1994), Criteria for identifying structures related to true crustal extension in orogens, *J. Struct. Geol.*, *16*, 1023–1027.

White, R. E. (1991), Properties of instantaneous seismic attributes, *Leading Edge*, *10*, 26–32.

Wu, R.-S., and K. Aki (1988), Introduction: Seismic wave scattering in three-dimensionally heterogeneous Earth, *Pure Appl. Geophys.*, *128*, 1–6.

Zamoshnyaya, N., and A. Suleimanov (2003), Final report of FIRE deep reflection survey carried out in Finland during 2001–2003, Spetzgeofizika, Moscow, Contract report, Volumes *I–II*.